

**Organic Batteries**

 How to cite: *Angew. Chem. Int. Ed.* **2023**, 62, e202214927

International Edition: doi.org/10.1002/anie.202214927

German Edition: doi.org/10.1002/ange.202214927

# Combining Deep Eutectic Solvents with TEMPO-based Polymer Electrodes: Influence of Molar Ratio on Electrode Performance\*\*

Matthias Uhl, Tanja Geng, Philipp A. Schuster, Benjamin W. Schick, Matthias Kruck, Alexander Fuoss, Alexander J. C. Kuehne, and Timo Jacob\*

**Abstract:** For sustainable energy storage, all-organic batteries based on redox-active polymers promise to become an alternative to lithium ion batteries. Yet, polymers contribute to the goal of an all-organic cell as electrodes or as solid electrolytes. Here, we replace the electrolyte with a deep eutectic solvent (DES) composed of sodium bis(trifluoromethanesulfonyl)imide (NaTFSI) and *N*-methylacetamide (NMA), while using poly(2,2,6,6-tetramethylpiperidin-1-yl-oxyl methacrylate) (PTMA) as cathode. The successful combination of a DES with a polymer electrode is reported here for the first time. The electrochemical stability of PTMA electrodes in the DES at the eutectic molar ratio of 1:6 is comparable to conventional battery electrolytes. More viscous electrolytes with higher salt concentration can hinder cycling at high rates. Lower salt concentration leads to decreasing capacities and faster decomposition. The eutectic mixture of 1:6 is best suited uniting high stability and moderate viscosity.

## Introduction

The development of new types of batteries (e.g. organic batteries) is driven by the need to address the climate crisis by strengthening non-fossil energy sources and compensating for net-fluctuations that renewable energy sources entail - since wind, sun, and tides are not synchronized with our demand for energy.<sup>[1-3]</sup> While full organic batteries are currently only foreseen as a niche technology,<sup>[4]</sup> many organic polymers are already used in electrochemical storage systems, such as lithium ion batteries. Applications include polymer separators and binders, polymer electrolytes, and polymers as redox-active materials in battery electrodes.<sup>[5]</sup> A wide variety of classes of redox-active polymers are investigated, including organosulfur polymers, conjugated polymers, and organic radical polymers.<sup>[6]</sup>

Although the application of DESs has been extended to battery application, e.g. in lithium ion batteries,<sup>[7-9]</sup> they have not been used as electrolytes in organic batteries yet. DESs as a class of non-aqueous electrolytes were originally introduced by Abbott and co-workers as catalysts for organic synthesis.<sup>[10]</sup> They nowadays find wide application also in extraction and separation<sup>[11,12]</sup> as well as electrochemical metal deposition.<sup>[13-15]</sup> If two components are mixed in their eutectic ratio, the binary mixture exhibits a freezing point depression caused by complexation mainly through hydrogen bonding, interactions between Lewis acids and bases and van der Waals interactions.<sup>[16]</sup> Depending on the composition, four different types of DESs can be distinguished. According to Smith and co-workers, DESs type I are composed of a metal salt mixed with an organic salt like a quaternary ammonium salt. The second type includes hydrated metal halides instead of the water-free ones in the previous case. DESs type III are mixtures of organic salts with hydrogen bond donors like alcohols or amides not including any metal cations. For DESs type IV, metal salts are mixed with hydrogen bond donors.<sup>[13]</sup> Both types III and IV are highly variable in their composition and therefore tunable in their physical and electrochemical behavior. Especially DESs type III are typically considered as green alternatives to ionic liquids and common solvents, since most of the DESs' components are non-toxic and environmentally-friendly.<sup>[13,17]</sup> Additionally, most DESs are non-flammable, exhibit low vapor pressures and wide electrochemical stability windows compared to water, enabling them to be promising candidates for battery electrolytes.<sup>[9]</sup>

[\*] M. Uhl, T. Geng, B. W. Schick, M. Kruck, A. Fuoss, Prof. Dr. T. Jacob  
 Institute of Electrochemistry, Ulm University  
 Albert-Einstein-Allee 47, 89081 Ulm (Germany)  
 E-mail: timo.jacob@uni-ulm.de

P. A. Schuster, Prof. Dr. A. J. C. Kuehne  
 Institute of Organic and Macromolecular Chemistry, Ulm University  
 Albert-Einstein-Allee 11, 89081 Ulm (Germany)

Prof. Dr. T. Jacob  
 Helmholtz-Institute Ulm (HIU) for Electrochemical Energy Storage  
 Helmholtzstr. 11, 89081 Ulm (Germany)  
 and  
 Karlsruhe Institute of Technology (KIT)  
 P.O. Box 3640, 76021 Karlsruhe (Germany)

[\*\*] A previous version of this manuscript has been deposited on a preprint server (<https://doi.org/10.26434/chemrxiv-2022-qj35z-v2>).

© 2022 The Authors. Angewandte Chemie International Edition published by Wiley-VCH GmbH. This is an open access article under the terms of the Creative Commons Attribution Non-Commercial NoDerivs License, which permits use and distribution in any medium, provided the original work is properly cited, the use is non-commercial and no modifications or adaptations are made.

To test the application of DESs as electrolytes for polymer electrodes, the well-investigated polymer PTMA, with a polymethacrylate backbone and stable 2,2,6,6-tetramethylpiperidin-1-yl-oxyl (TEMPO) radicals in the periphery, serves as model system. More than 20 years ago, PTMA has been presented for the first time as a material for energy storage in rechargeable batteries. The fabricated batteries have demonstrated an average discharge voltage of 3.5 V and a discharge capacity of 77 Ah kg<sup>-1</sup> using Li as battery anode.<sup>[18,19]</sup> Further work improved the properties of PTMA electrodes by optimizing the carbon black and binder content in composite electrodes and by reducing the PTMA particle size by milling.<sup>[20]</sup> Customized changes in morphology can also be achieved by emulsion polymerization of PTMA. The resulting spherical particles, which can be controlled in size by the experimental conditions, exhibit a large surface area and are well applicable in composite electrodes.<sup>[21]</sup> Beside particles, PTMA brush polymers are of great interest today showing improvements especially in high-rate performance.<sup>[22]</sup> Since 2011, TEMPO radicals are also investigated for organic redox flow batteries.<sup>[23]</sup> Here, PTMA also works well as a redox-active compound in flow batteries, e.g. with a TEMPO derivative as redox mediator.<sup>[24]</sup>

Both concepts, organic polymer electrodes and deep eutectic solvents, aim for environmentally-friendly and sustainable future energy storage. However, DESs as electrolytes have not yet been combined with organic redox-active polymers, obviating understanding and transfer of these systems into application. In the present study, we show that DESs can indeed serve as suitable electrolytes for all-organic batteries with redox-active polymer electrodes. We go beyond the proof-of-concept by investigating the influence of the molar composition of the DES in detail, finding a high influence on the electrochemical stability, activity, and high-rate performance of the redox-active polymer. Among several mixtures, the eutectic mixture of the used DES is highlighted.

Since PTMA is well investigated in several electrolytes showing high stability and activity, it is used as active material in the polymer electrodes. The utilized DES type IV consists of NaTFSI and NMA, which has been selected because of its high electrochemical stability in the potential region of interest. Common DESs type III cannot fulfill this requirement of high anodic stability.<sup>[25]</sup> Additionally, this electrolyte is non-corrosive towards the aluminium current collector. Several mixtures of NaTFSI and NMA in different molar ratios were already physically characterized by De Sloovere and co-workers.<sup>[26]</sup> Their studies based on Raman and nuclear magnetic resonance spectroscopy and measurements of ionic conductivity, viscosity and thermal stability show the replacement of hydrogen bonds between NMA molecules by ionic bonds with increasing salt concentration. This leads to lower ionic conductivity and higher viscosity. The results are in agreement with their theoretical calculations on a molecular level. Despite a special complexation behavior for a DES in its eutectic composition is known,<sup>[27]</sup> no discontinuities of these experimentally determined physical properties were observed which would indicate the

eutectic ratio and special characteristics of the eutectic mixture.

In this study, we identified the eutectic composition of NaTFSI:NMA as 1:6 with the help of differential scanning calorimetry (DSC) measurements. Determination of the viscosity and density of the different mixtures including explicitly the eutectic one does as well not show outstanding behavior of the 1:6 mixture. This is different for the electrochemical performance of the PTMA electrodes in contact with the DES mixtures. Cyclic voltammetry (CV) and galvanostatic charge-discharge cycling in half cells highlight the eutectic ratio as the best choice in terms of stability and activity among the tested mixtures. This is explained by the complexation structure in NaTFSI:NMA 1:6. To identify the electrochemical stability window of the electrolytes, linear sweep voltammetry (LSV) on graphite electrodes is used.

## Results and Discussion

### Thermal Characterization of the DES

To determine the eutectic composition of mixtures consisting of NaTFSI and NMA, DSC measurements of various mixtures in different molar ratios are performed. The heating curve of each sample has been recorded from -180 °C to 80 °C with a heating rate of 1 °C min<sup>-1</sup>, as shown in Figure 1A in the relevant temperature range. Between 100 °C and 250 °C, NMA is evaporating followed by thermal decomposition of NaTFSI at temperatures higher than 360 °C.<sup>[26]</sup> Below -50 °C, the DSC curves exhibit a step in the baseline corresponding to the glass transition. Since the samples have been cooled fast before the depicted heating step, recrystallization occurs upon heating causing exothermic peaks. If the temperature is increased further, the samples melt and endothermic peaks are observable. The relatively slow heating rate is chosen to achieve a better separation of the recrystallization and melting events, so that the melting enthalpies can be reliably determined, while still being able to analyze the glass transitions.

The glass transition temperature of each curve is determined by the temperature of a tangent to the step itself at half height of the step. Thereby, the enthalpic recovery, visible as a small endothermic peak at the end of the glass transition, is not considered. The glass transition temperature increases linearly with increasing amount of NaTFSI for molar ratios of  $x_{\text{NaTFSI}} \geq 0.09$ , as shown in Figure 1B in red.

To determine the eutectic ratio of the NaTFSI:NMA DES, the melting peaks are analyzed. Normally, one would expect two melting peaks for each sample with one occurring at the same temperature independently of the composition. This peak would correspond to the melting of the eutectic and therefore, one could obtain the solidus curve of the phase diagram and from that, the eutectic temperature. For example, this is the case for various DESs type III, whose eutectic temperature has been determined accordingly.<sup>[14,28]</sup> However, similar behavior is not observed

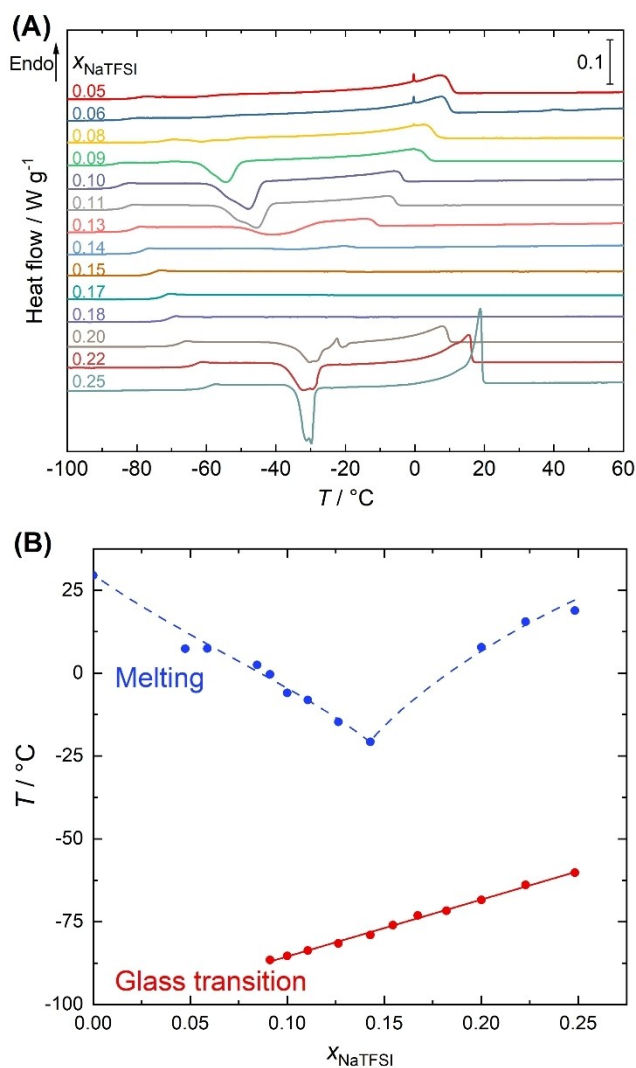


**Figure 1.** A) DSC curves of NaTFSI:NMA mixtures in various compositions recorded with a heating rate of  $1\text{ °C min}^{-1}$ . The endothermic heat flow is shown as a function of temperature in the relevant range and for better readability, the thermograms are shifted against each other. B) Phase diagram of the NaTFSI:NMA DES as a function of the mole fraction of NaTFSI. The glass transition temperatures (red) are fitted with a linear fit. The temperatures of the melting peak (blue) are approximated by the dashed line as guide for the eye.

for the NaTFSI:NMA mixtures (Figure 1A). We assume that this mixture does not crystallize and subsequently cannot melt. Instead, it is forming a glass and therefore, only the glass transition is observable. The second melting event is expected to take place at a higher temperature depending on the composition and corresponding to melting of the excess component, thus yielding the liquidus curve. As only one melting event occurs at variable temperatures for the NaTFSI:NMA DES, we assume that it corresponds to melting of the respective excess component. The melting temperatures leading to the liquidus curve are determined as the peak temperatures because at the peak, the excess component in each sample has molten completely and the whole mixture will be liquid. Therefore, the melting peak

temperatures of the different samples are given in Figure 1B in blue as a function of composition.

The melting temperature first decreases with increasing amount of NaTFSI until  $x_{\text{NaTFSI}} = 0.14$ . The mixtures with  $0.15 \leq x_{\text{NaTFSI}} \leq 0.18$  exhibit no processes other than the glass transition, but for  $x_{\text{NaTFSI}} \geq 0.2$  the melting temperatures increase with NaTFSI content. This leads to a minimum at  $x_{\text{NaTFSI}} = 0.14$ , which is a good estimate for the eutectic composition and corresponds to a NaTFSI:NMA ratio of about 1:6. Further evidence for this ratio can be found in a plot of the melting enthalpies as a function of the molar ratio (Figure S1). If the melting peak corresponds to melting of the excess component, it should exhibit a higher enthalpy, the more the ratio deviates from the eutectic ratio. Therefore, we expect a minimum at the eutectic ratio, which is at  $x_{\text{NaTFSI}} = 0.15$  (NaTFSI:NMA 1:5.8), a ratio very similar to the one determined from the DSC curves themselves. The number of six NMA molecules per NaTFSI matches the theoretical calculations of De Sloovere and co-workers for different mixtures in the liquid phase.<sup>[26]</sup> If enough NMA is present,  $\text{Na}^+$  and  $\text{TFSI}^-$  bind to three NMA molecules each via ionic or hydrogen bonds, respectively. In case of  $\text{TFSI}^-$ , structures with more NMA molecules are as well possible. In case of high salt concentration, ionic bonds between the ions replace the hydrogen bonds with NMA.<sup>[26]</sup> From that point of view, the eutectic ratio of 1:6 appears coherent.

NaTFSI:NMA mixtures without recrystallization and melting have also been observed previously in DSC experiments with a heating rate of  $10\text{ °C min}^{-1}$ .<sup>[26]</sup> The same is true for mixtures of LiTFSI with different sulfonamide-based hydrogen bond donors.<sup>[29]</sup> In a LiTFSI:NMA DES, a glass transition and a melting peak dependent on the molar ratio have been observed by DSC measurements.<sup>[8,30]</sup> For a LiTFSI molar ratio between 0.15 and 0.2, only a glass transition occurs, which is analogous to our observations using NaTFSI. In the case of LiTFSI, a eutectic ratio of  $x_{\text{LiTFSI}} = 0.2$  and a eutectic temperature of  $-72\text{ °C}$  have been reported, whereby the latter corresponds to the glass transition temperature of the eutectic mixture.<sup>[8]</sup> For this DES, a eutectic ratio of  $x_{\text{LiTFSI}} = 0.17$  has been calculated theoretically.<sup>[7]</sup>

As there are several ratios with LiTFSI as well as NaTFSI without melting peak, the eutectic ratio can only be estimated, as described before. Since one cannot be entirely sure about the exact course of the liquidus curve and since the solidus curve is not observed, no conclusion is drawn about the eutectic temperature of the NaTFSI:NMA DES. However, with a large freezing-point depression of the eutectic mixture ( $x_{\text{NaTFSI}} = 0.14$ , NaTFSI:NMA 1:6) of more than  $50\text{ °C}$  with respect to the melting point of pure NMA, NaTFSI:NMA is clearly a DES. For the mixtures with  $x_{\text{NaTFSI}} \leq 0.06$ , a small endothermic peak appears around  $0\text{ °C}$  (Figure 1A), which is also observable in pure NMA (Figure S2) and has been detected previously.<sup>[26]</sup> It is probably connected to the residual water content of undried NMA.

## Electrochemical Characterization

In the next step, we investigated the applicability of DESs as electrolytes in all-organic batteries. The DES NaTFSI:NMA in its eutectic composition is combined with well-investigated polymer electrodes based on PTMA as redox-active material<sup>[21]</sup> and compared with mixtures with higher and lower salt concentration. The fabrication of the electrodes is described in the experimental section. The influence of the molar composition of the DES on the electrochemical behavior of PTMA electrodes is analyzed using the before-mentioned DES in several molar ratios. The quality and performance of the self-made electrodes are comparable to those of Muench and co-workers<sup>[21]</sup> since the electrochemical behavior and the specific capacity of the electrodes in 1 M 1-butyl-1-methylpyrrolidinium bis(trifluoromethylsulfonyl)imid (Pyr<sub>14</sub>TFSI) in propylene carbonate are almost identical (Figures S3 and S4). The oxidation of the TEMPO radical units and the reduction in the reverse scan direction is taking place at approximately 600 mV vs. Ag pseudo reference electrode. The maximum specific discharge capacity is roughly 94 mAh g<sup>-1</sup> based on the mass of PTMA.

Using the DES NaTFSI:NMA instead of the propylene carbonate-based electrolyte for cyclic voltammetry in half-cells with PTMA electrodes (Figure 2), the oxidation and reduction of the TEMPO units is also observed at potentials around 600 mV vs. Ag. Small deviations in the redox potential are caused by minor instabilities of the pseudo reference electrode. The usage of real reference electrodes is opposed since the Swagelok-type cell setup allows symmetric and reproducible assembly of the electrodes and separators only with wire-shaped reference electrodes. The Ag wire turned out to be stable during a measurement and only showed acceptable deviations in the range of several millivolts at different days. The peaks in the cyclic voltammograms of the PTMA electrode in the DESs exhibit smaller peak currents but a slower current decay after reaching the maximum current than in the case of the carbonate-based electrolyte (Figure S3). Positive of 1 V vs. Ag, irreversible oxidation occurs, most likely caused by anodic decomposition of the electrolyte. According to Figure 2C and the LSV curves in Figure S5, this is more pronounced for DESs with lower amounts of NaTFSI. High decomposition currents appear at potentials above 1.5 V vs. Ag in all cases with the starting potential shifting to higher values with increasing salt concentration. However, already at lower potentials, decomposition currents of NaTFSI:NMA 1:12 are higher than for the 1:6 and 1:4 mixtures. The difference becomes significant at potentials higher than 1 V.

Additionally, there is a significant difference in the initial activity between electrolytes with salt concentrations higher than or equal to the eutectic mixture (Figures 2A and B) and those with lower salt contents (Figures 2C and S6). For high salt concentrations, peak currents are increasing within the first cycles after assembling and equilibrating the electrochemical cell for 5 hours. This behavior is more pronounced in the 1:4 mixture than in the eutectic mixture of 1:6. Lower concentrated electrolytes cause high currents

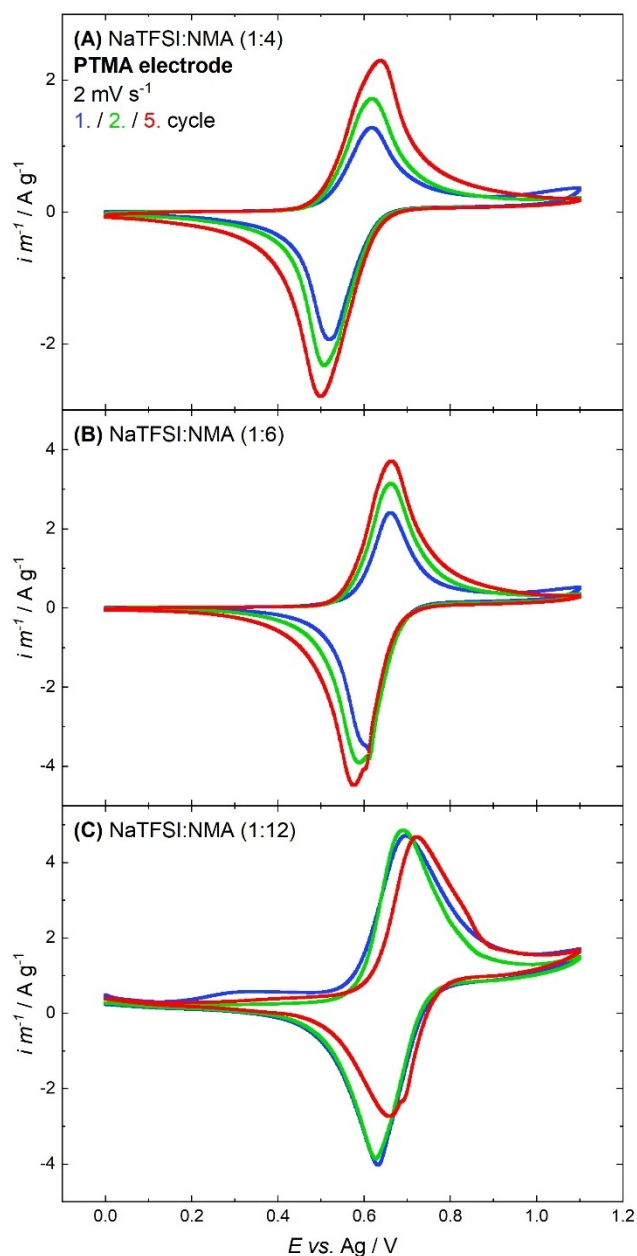


**Figure 2.** Cyclic voltammograms of PTMA electrodes in NaTFSI:NMA DESs with a molar ratio of A) 1:4, B) 1:6, and C) 1:12 showing the 1<sup>st</sup> (blue), 2<sup>nd</sup> (green), and 5<sup>th</sup> (red) cycle at a scan rate of 2 mV s<sup>-1</sup>.

right from the beginning, which are in some cases accompanied with a quite large irreversible oxidation in the initial cycle (Figure S6). In contrast to the DESs with high salt concentration, especially cathodic currents are rather decreasing during cycling.

To unravel the origin of the differences in the cyclic voltammograms (Figure 2), viscosity and density of various mixtures were measured at different temperatures. In Figure 3, the dynamic viscosity  $\eta$  at 20 °C, 25 °C, 40 °C, and 80 °C is shown as a function of the molar ratio of NaTFSI. It is evident that the higher the salt content, the higher is the viscosity, and there is no exception for the eutectic 1:6

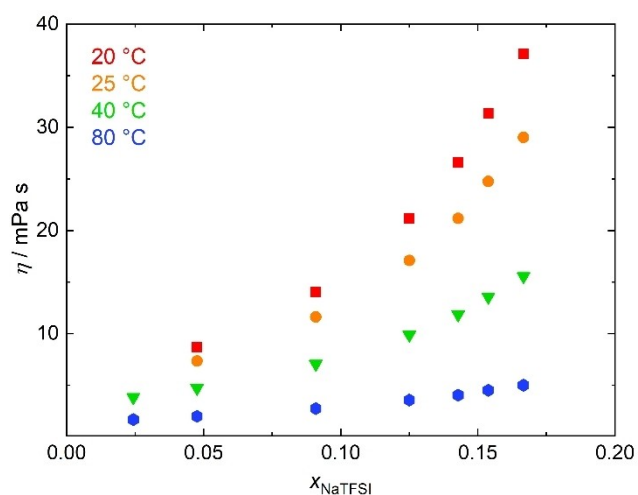


**Figure 3.** Dynamic viscosity at 20 °C (red), 25 °C (orange), 40 °C (green), and 80 °C (blue) for NaTFSI:NMA mixtures in different molar ratios.

mixture ( $x_{\text{NaTFSI}} = 0.14$ ). Moreover, lower temperatures entail higher viscosities. Further evaluation of the viscosity and density is given in the Supporting Information (Figures S7 and S8).

Referring to the high viscosity of DESs at room temperature at the eutectic composition and with higher salt concentration, the initial increase in capacity during cycling could be caused by a disadvantageous wetting behavior compared to less viscous electrolytes. The time to wet and infiltrate the internal surface of smaller pores of the electrode with electrolyte may be longer especially since the unipolar polymer chains interact stronger with neutral NMA molecules than with the dissolved salt. This leads to disabled electrolyte contact for parts of the active material and with this to initially lower capacities.<sup>[31,32]</sup>

After these initial cycles, voltammograms are recorded at a higher scan rate to monitor the cycling stability (Figure 4). Here, the advantage of highly-concentrated electrolytes is clearly observable. With mixtures in the molar ratio 1:4 and 1:6 (Figures 4A and B), PTMA exhibits excellent cycling stability for 100 cycles. The peak shape and peak current densities remain almost unchanged over the whole period. In this case, the investigated DESs perform equally good as the electrolyte based on propylene carbonate (Figure S9).

For lower salt concentrations (Figures 4C and S10), the cycling stability changes dramatically. Already during the first cycles, the currents caused by the oxidation of the TEMPO radical decrease continuously, whereas the decomposition currents at the positive end of the potential stability window remain unaffected, indicating continuous degradation.

The reason for the high electrochemical stability of the DES in its eutectic ratio and at higher salt concentrations is the strong interaction between the ions and the NMA molecules in the DES mixtures. A high concentration of ions in the electrolyte leads to complexed supramolecular network-like 3D-structures in the liquid. Through mainly

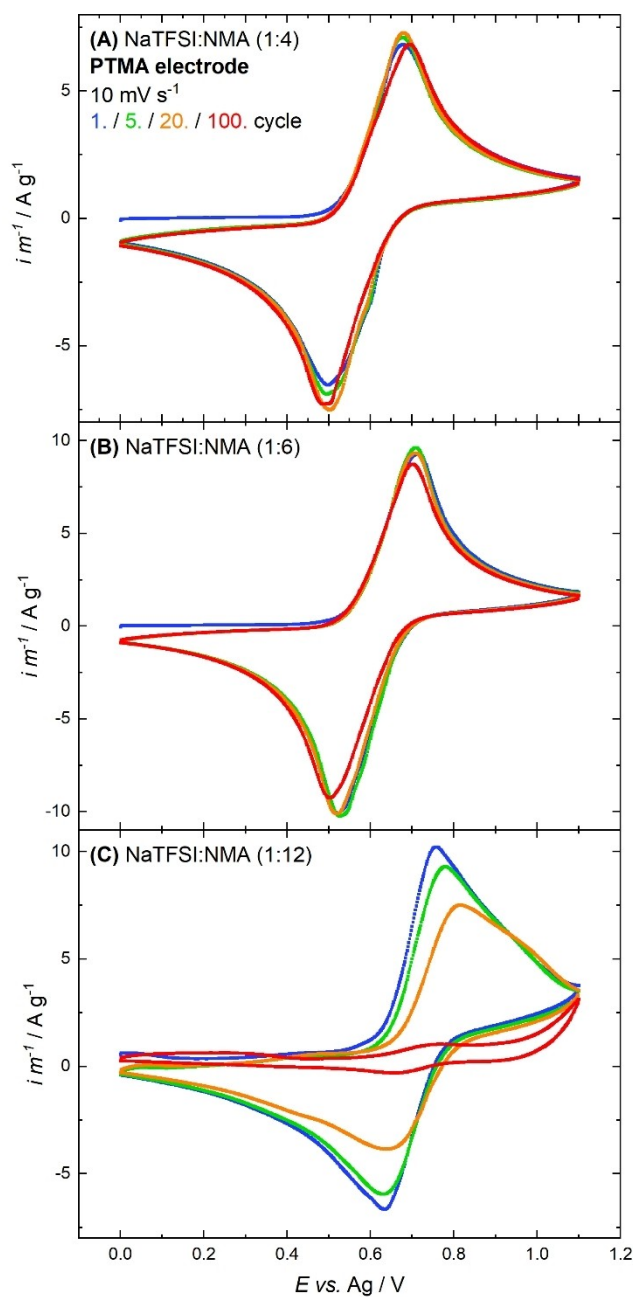


**Figure 4.** Cyclic voltammograms of PTMA electrodes in NaTFSI:NMA DESs with a molar ratio of A) 1:4, B) 1:6, and C) 1:12 at a scan rate of 10 mV s<sup>-1</sup> to test the cycling stability. The 1<sup>st</sup> (blue), 5<sup>th</sup> (green), 20<sup>th</sup> (orange), and 100<sup>th</sup> (red) cycle are shown.

hydrogen and ionic bonding, reactive groups of the molecules are stabilized and therefore protected from decomposition reactions. This is also reflected in a decrease in energy of the HOMO of the solvent.<sup>[33,34]</sup> For DESs, this is equally valid. Hammond and co-workers found such complexed network-like layered structures in a DES composed of choline chloride and urea in its eutectic composition showing that all ions and solvent molecules are taking part in the complexation.<sup>[27]</sup> For the DES NaTFSI:NMA used in this study, De Sloovere and co-workers also found a

stabilizing effect by high salt concentrations experimentally, as well as by calculating the HOMO energies with density functional theory. Because of the decrease in HOMO energy, the anodic stability of NMA increases.<sup>[26]</sup> Based on the knowledge of the complexation in DESs in their eutectic ratio,<sup>[27]</sup> we conclude that in the eutectic mixture of NaTFSI:NMA 1:6, all ions and NMA molecules are complexed and therefore stabilized leading to high cycling stability and low decomposition currents. In DESs with lower salt concentrations than the eutectic ratio, non-complexed or not fully complexed NMA molecules are less stable causing continuous electrolyte decomposition at potentials higher than 1 V.

Nevertheless, a specific reason for the capacity fading in lower-concentrated DESs cannot be given for granted. Possibly, the excess solvent slowly dissolves PTMA, thus reducing the amount of redox-active material on the electrode. At least this is known to happen for structurally similar radical-polymers in carbonate solvents.<sup>[35]</sup> However, in case of PTMA in a highly-concentrated DES and in a propylene carbonate electrolyte, the capacities in cyclic voltammetry and the macroscopic appearance of the electrodes remain unchanged. An alternative explanation is that decomposition products of the non-complexed NMA molecules could block active sites on the PTMA electrodes either by reacting with the radical or the cationic group of the PTMA itself or by covering the electrode surface with an insoluble non-conductive organic film. The blocking of pores by decomposition products of organic electrolytes is reported e.g. by Azaïs and co-workers.<sup>[36]</sup> Scanning electron microscopy (SEM) of an electrode which was cycled first with 2 mVs<sup>-1</sup> and afterwards with 10 mVs<sup>-1</sup> in NaTFSI:NMA 1:12 in the same potential range as for the electrochemical characterization in Figure 2C and 4C does not provide evidence for the evolution of a thick passivation layer on the electrode surface (Figure S11). This is especially true if it is compared to an electrode that was held at OCP for the same time, as there are no differences. Therefore, the specific reason for the capacity fading remains unclear.

### Galvanostatic Cycling

To get an insight into the behavior of PTMA as active material in battery cathodes, galvanostatic charge-discharge measurements with a rate of 10 C were performed using the same electrochemical setup as for cyclic voltammetry. Since PTMA is commonly used as a cathode material for batteries,<sup>[22,37,38]</sup> the oxidation of the TEMPO radicals is defined as the charging step and the accompanying reduction corresponds to discharging. To calculate the Coulombic efficiency *CE*, the specific discharge capacity  $C_{sp,dc}$  is divided by the specific charge capacity  $C_{sp,c}$  of the same cycle *n* (Equation 1).

$$CE = \frac{C_{sp,dc}(n)}{C_{sp,c}(n)} \quad (1)$$

The capacity retention *CR* is defined by the specific discharge capacities of two following cycles (Equation 2).<sup>[39]</sup>

$$CR = \frac{C_{sp,dc}(n+1)}{C_{sp,dc}(n)} \quad (2)$$

As discussed before, the salt concentration in the DES has a significant influence on the initial capacity as well as long-term electrochemical stability and activity. This is also true for the galvanostatic measurements (Figure 5). For the DES in its eutectic ratio of 1:6, the specific capacity increases in the first charging steps just as observed by cyclic voltammetry (Figure 2B), leading to a capacity retention higher than 1 in the beginning. After reaching a limit of roughly 70 mAhg<sup>-1</sup> after 10 cycles, the Coulombic efficiency stabilizes at around 97%. It is accompanied by a capacity retention of more than 99% leading to a slowly decreasing specific capacity. Compared to the electrochemical long-term stability in cyclic voltammetry, PTMA exhibits a little higher capacity loss in galvanostatic measurements. After 100 cycles, the capacity reaches approximately 70% of the maximum value. One factor for this more prominent capacity fading is the measurement time. Hundred galvanostatic charge-discharge cycles with a rate of 10 C last up to 20 hours and take therefore roughly three times longer than 100 cycles in CV at 10 mVs<sup>-1</sup>. If dissolution of neutral or charged PTMA is meant to be the reason for decreasing capacities, this effect of time is rather relevant.

For the DESs with lower salt concentration, the electrochemical behavior during charge-discharge cycling is comparable to the previous findings with cyclic voltammetry (Figures 4C and S10). Already in the initial cycle, the maximum specific discharge capacity is achieved followed by a faster decrease in capacity than for the eutectic mixture. The Coulombic efficiency is lower than 90% indicating an irreversible oxidation process which is also observed in the cyclic voltammograms (Figures 4C and S10). The capacity retention of 98–99% reflects the continuous decrease in capacity. High irreversible currents are observed for the initial charging step, as seen by cyclic voltammetry (Figure S6). This phenomenon can be associated with electrolyte decomposition.<sup>[40]</sup>

Because of the high rates for charging and discharging, the maximum specific discharge capacity of the PTMA electrodes is around 70 mAhg<sup>-1</sup> for all tested DESs. For a lower rate of 1.5 C in the DES at the eutectic mixture (Figure S12A), the maximum specific discharge capacity is roughly 30% higher. This is in agreement with half-cell tests of PTMA electrodes of Muench and co-workers in a carbonate-based electrolyte,<sup>[21]</sup> which is able to achieve efficient and stable cycling of PTMA electrodes even at 10 C (Figure S4).

Surprisingly, it is not possible to achieve efficient galvanostatic charging and discharging with NaTFSI:NMA 1:4 at a rate of 10 C. At such high currents, the measured capacities are far below the expected values. The potential profiles do not show a clear potential plateau at the expected value of 0.6 V. Therefore, NaTFSI:NMA 1:4 is unsuited for charging and discharging at high rates. The reason for this seems to be the high viscosity. Beside the disadvantageous wetting of the electrodes,<sup>[31,32]</sup> high salt

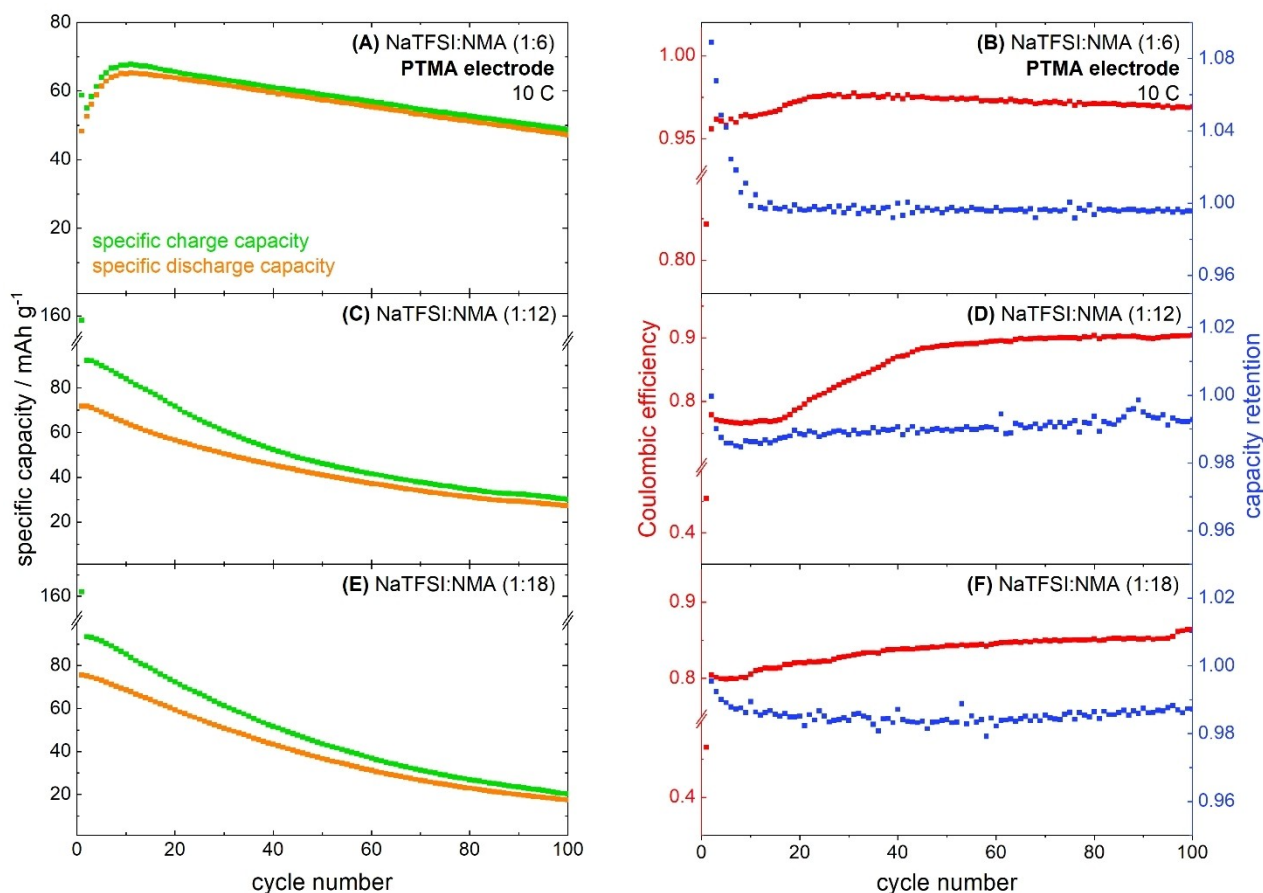


**Figure 5.** Chronopotentiometric charge-discharge cycling of PTMA electrodes in NaTFSI:NMA DESs with a molar ratio of A, B) 1:6, C, D) 1:12, and E, F) 1:18 between 0 V and 1 V vs. Ag at a rate of 10 C. A, C, E) Specific charge (green) and discharge (orange) capacities for 100 cycles; B, D, F) corresponding Coulombic efficiency (red) and capacity retention (blue).

concentrations can hinder salt dissociation and lower the ionic conductivity of the electrolyte.<sup>[26]</sup> This is also reflected in the comparably high Ohmic resistance of 25  $\Omega$  for the 1:4 mixture compared to lower concentrated DESs (Figure S13). While DESs with ratios of 1:12 and 1:18 show nearly the same resistance of the electrolyte with  $\approx 15 \Omega$ , the resistance of the eutectic ratio is already a little higher (17  $\Omega$ ). The 1:4 mixture clearly leads to the highest resistance, even though the salt concentration is only little higher than in the eutectic ratio. This fact again highlights the role of the eutectic composition.

At 1.5 C and after a dwell time of 70 h, NaTFSI:NMA 1:4 exhibits an improved performance. The Coulombic efficiency is relatively high (97.5%), accompanied by a capacity retention close to 1 (Figures S12A and B). The maximum specific discharge capacity reaches an overall limit of 90  $\text{mAhg}^{-1}$ , which is close to the capacity determined in the propylene carbonate-based electrolyte (Figure S4). Within 100 cycles, the capacity decreases by more than 50% in total for the highly-concentrated DES.

With the eutectic mixture NaTFSI:NMA 1:6, the electrochemical activity of PTMA decreases faster than for more concentrated DES (Figures S12C and D). This is most likely attributed to the higher share of NMA as discussed

before. It is noteworthy to mention, that after the long dwell time of 70 h, the maximum discharge capacity of 87  $\text{mAhg}^{-1}$  is achieved directly in the first cycle and no further activation is needed. This also indicates that PTMA is not dissolved or passivated before the first oxidation. More likely, the cationic TEMPO-moieties dissolve or react, thereby leading to decreasing capacities during cycling which is more relevant when using low cycling rates.

## Conclusion

In this study, we proved the successful combination of DESs with polymer electrodes paving the way to a new type of sustainable all-organic batteries. In this regard, the DES NaTFSI:NMA was characterized by DSC finding the eutectic ratio at 1:6. Despite there is no exception in the physical behavior of the NaTFSI:NMA mixtures in different molar ratios, the electrochemical properties of the eutectic composition stand out. Applied as electrolytes for redox-active PTMA electrodes, the composition of the DES highly affects the electrochemical performance of the half-cells. The two opposing trends of lower ionic conductivity through ion pairing and higher anodic stability due to decreasing

HOMO energies of NMA by increasing salt concentration find their best compromise in the eutectic mixture. Since all solvent molecules are taking part in the complexation of the ions in the eutectic mixture, oxidation of less stable free NMA molecules is prevented. On the other hand, ion pairing is avoided by providing enough solvent molecules leading to higher ionic conductivity and lower viscosity than for DESs with even higher salt concentration. This enables good wettability and conductivity for the eutectic mixture of NaTFSI:NMA while maintaining the stability of the electrolyte. Coulombic efficiencies of 97 % are achieved in galvanostatic charge-discharge cycling of the PTMA half-cells at a rate of 10 C. The electrochemical stability is even better when using cyclic voltammetry reflecting the compatibility of the DES with PTMA electrodes.

With this work, the applicability of DESs for future energy storage in all-organic batteries as sustainable alternative has been proven successfully. The importance and advantage of using the DES in its eutectic ratio has been discussed in detail. In terms of environmental friendliness, the use of DESs type III would even be more advantageous than the here investigated DESs type IV. However, current DESs type III exhibit poor anodic stability at the oxidation potential of PTMA. For future studies, the combination of DESs and redox-active polymers need to be chosen carefully to match the electrochemical stability window of the electrolyte with the redox potential of the polymer. Additionally, other factors such as viscosity of the electrolyte and solubility of the active material in the electrolyte are crucial parameters for a well-performing organic battery.

### Author Contributions

M. Uhl: Conceptualization, Formal Analysis, Investigation, Validation, Visualization, Writing—Original Draft Preparation; T. Geng: Conceptualization, Formal Analysis, Investigation, Validation, Visualization, Writing—Original Draft Preparation; P. A. Schuster: Investigation, Writing—Original Draft Preparation; B. W. Schick: Conceptualization, Writing—Review & Editing; M. Kruck: Investigation, Writing—Review & Editing; A. Fuoss: Investigation; A. J. C. Kuehne: Funding Acquisition, Resources, Supervision, Writing—Review & Editing; T. Jacob: Funding Acquisition, Resources, Supervision, Writing—Review & Editing.

### Acknowledgements

We thank Dr. Simon Muench and Prof. Dr. Ulrich Schubert for providing PTMA particles for the investigated polymer electrodes. We also thank Evelyn Artmann for recording SEM images of the self-made electrodes. This work contributes to the research performed at CELEST (Center for Electrochemical Energy Storage Ulm-Karlsruhe) and we thank the German Research Foundation (DFG) for funding under Project ID 390874152 (POLiS Cluster of Excellence), and for funding within the priority program SPP 2248

Polymer-based Batteries (Project ID 441209207). Open Access funding enabled and organized by Projekt DEAL.

### Conflict of Interest

The authors declare no conflict of interest.

### Data Availability Statement

The data that support the findings of this study are available from the corresponding author upon reasonable request.

**Keywords:** Deep Eutectic Solvent · Electrochemistry · Organic Battery · PTMA Electrode · Sustainable Chemistry

- [1] D. Larcher, J.-M. Tarascon, *Nat. Chem.* **2015**, *7*, 19–29.
- [2] J. Kim, J. H. Kim, K. Ariga, *Joule* **2017**, *1*, 739–768.
- [3] N. Goujon, N. Casado, N. Patil, R. Marcilla, D. Mecerreyes, *Prog. Polym. Sci.* **2021**, *122*, 101449.
- [4] J. P. Esquivel, P. Alday, O. A. Ibrahim, B. Fernández, E. Kjeang, N. Sabaté, *Adv. Energy Mater.* **2017**, *7*, 1700275.
- [5] D. Mecerreyes, L. Porcarelli, N. Casado, *Macromol. Chem. Phys.* **2020**, *221*, 1900490.
- [6] S. Muench, A. Wild, C. Friebe, B. Häupler, T. Janoschka, U. S. Schubert, *Chem. Rev.* **2016**, *116*, 9438–9484.
- [7] W. Zaidi, A. Boisset, J. Jacquemin, L. Timperman, M. Anouti, *J. Phys. Chem. C* **2014**, *118*, 4033–4042.
- [8] A. Boisset, S. Menne, J. Jacquemin, A. Balducci, M. Anouti, *Phys. Chem. Chem. Phys.* **2013**, *15*, 20054.
- [9] J. Wu, Q. Liang, X. Yu, Q. Lü, L. Ma, X. Qin, G. Chen, B. Li, *Adv. Funct. Mater.* **2021**, *31*, 2011102.
- [10] A. P. Abbott, G. Capper, D. L. Davies, H. L. Munro, R. K. Rasheed, V. Tambyrajah, *Chem. Commun.* **2001**, 2010–2011.
- [11] X. Li, K. H. Row, *J. Sep. Sci.* **2016**, *39*, 3505–3520.
- [12] M. Ruesgas-Ramón, M. C. Figueroa-Espinoza, E. Durand, *J. Agric. Food Chem.* **2017**, *65*, 3591–3601.
- [13] E. L. Smith, A. P. Abbott, K. S. Ryder, *Chem. Rev.* **2014**, *114*, 11060–11082.
- [14] T. Geng, S. J. Zeller, L. A. Kibler, M. U. Cebelin, T. Jacob, *ChemElectroChem* **2022**, *9*, e202101283.
- [15] M. U. Cebelin, S. Zeller, B. Schick, L. A. Kibler, T. Jacob, *ChemElectroChem* **2019**, *6*, 141–146.
- [16] L. Geng, X. Wang, K. Han, P. Hu, L. Zhou, Y. Zhao, W. Luo, L. Mai, *ACS Energy Lett.* **2022**, *7*, 247–260.
- [17] B. B. Hansen, S. Spittle, B. Chen, D. Poe, Y. Zhang, J. M. Klein, A. Horton, L. Adhikari, T. Zelovich, B. W. Doherty, B. Gurkan, E. J. Maginn, A. Ragauskas, M. Dadmun, T. A. Zawodzinski, G. A. Baker, M. E. Tuckerman, R. F. Savinell, J. R. Sangoro, *Chem. Rev.* **2021**, *121*, 1232–1285.
- [18] K. Nakahara, S. Iwasa, M. Satoh, Y. Morioka, J. Iriyama, M. Suguro, E. Hasegawa, *Chem. Phys. Lett.* **2002**, *359*, 351–354.
- [19] H. Nishide, S. Iwasa, Y. J. Pu, T. Suga, K. Nakahara, M. Satoh, *Electrochim. Acta* **2004**, *50*, 827–831.
- [20] S. Komaba, T. Tanaka, T. Ozeki, T. Taki, H. Watanabe, H. Tachikawa, *J. Power Sources* **2010**, *195*, 6212–6217.
- [21] S. Muench, P. Gerlach, R. Burges, M. Strumpf, S. Hoepfner, A. Wild, A. Lex-Balducci, A. Balducci, J. C. Brendel, U. S. Schubert, *ChemSusChem* **2021**, *14*, 449–455.
- [22] R. Rohan, M.-K. Hung, Y.-F. Yang, C.-W. Hsu, C.-K. Yeh, Y.-L. Chang, J.-T. Lee, *ACS Appl. Polym. Mater.* **2022**, *4*, 2365–2372.

- [23] Z. Li, S. Li, S. Liu, K. Huang, D. Fang, F. Wang, S. Peng, *Electrochem. Solid-State Lett.* **2011**, *14*, A171.
- [24] E. Schröter, C. Stolze, A. Saal, K. Schreyer, M. D. Hager, U. S. Schubert, *ACS Appl. Mater. Interfaces* **2022**, *14*, 6638–6648.
- [25] R. Costa, M. Figueiredo, C. M. Pereira, F. Silva, *Electrochim. Acta* **2010**, *55*, 8916–8920.
- [26] D. De Sloovere, D. E. P. Vanpoucke, A. Paulus, B. Joos, L. Calvi, T. Vranken, G. Reekmans, P. Adriaensens, N. Eshraghi, A. Mahmoud, F. Boschini, M. Safari, M. K. Van Bael, A. Hardy, *Adv. Energy Sustainability Res.* **2022**, *3*, 2100159.
- [27] O. S. Hammond, D. T. Bowron, K. J. Edler, *Green Chem.* **2016**, *18*, 2736–2744.
- [28] X. Meng, K. Ballerat-Busserolles, P. Husson, J.-M. Andanson, *New J. Chem.* **2016**, *40*, 4492–4499.
- [29] O. E. Geiculescu, D. D. DesMarteau, S. E. Creager, O. Haik, D. Hirshberg, Y. Shilina, E. Zinigrad, M. D. Levi, D. Aurbach, I. C. Halalay, *J. Power Sources* **2016**, *307*, 519–525.
- [30] A. Boisset, J. Jacquemin, M. Anouti, *Electrochim. Acta* **2013**, *102*, 120–126.
- [31] R.-S. Kühnel, S. Obeidi, M. Lübke, A. Lex-Balducci, A. Balducci, *J. Appl. Electrochem.* **2013**, *43*, 697–704.
- [32] M.-S. Wu, T.-L. Liao, Y.-Y. Wang, C.-C. Wan, *J. Appl. Electrochem.* **2004**, *34*, 797–805.
- [33] J. Wang, Y. Yamada, K. Sodeyama, C. H. Chiang, Y. Tateyama, A. Yamada, *Nat. Commun.* **2016**, *7*, 12032.
- [34] K. Yoshida, M. Nakamura, Y. Kazue, N. Tachikawa, S. Tsuzuki, S. Seki, K. Dokko, M. Watanabe, *J. Am. Chem. Soc.* **2011**, *133*, 13121–13129.
- [35] K.-A. Hansen, J. Nerkar, K. Thomas, S. E. Bottle, A. P. O'Mullane, P. C. Talbot, J. P. Blinco, *ACS Appl. Mater. Interfaces* **2018**, *10*, 7982–7988.
- [36] P. Azaïs, L. Duclaux, P. Florian, D. Massiot, M.-A. Lillo-Rodenas, A. Linares-Solano, J.-P. Peres, C. Jehoulet, F. Béguin, *J. Power Sources* **2007**, *171*, 1046–1053.
- [37] K. Nakahara, J. Iriyama, S. Iwasa, M. Suguro, M. Satoh, E. J. Cairns, *J. Power Sources* **2007**, *165*, 398–402.
- [38] J. K. Kim, J. H. Ahn, G. Cheruvally, G. S. Chauhan, J. W. Choi, D. S. Kim, H. J. Ahn, S. H. Lee, C. E. Song, *Met. Mater. Int.* **2009**, *15*, 77–82.
- [39] A. Tornheim, D. C. O'Hanlon, *J. Electrochem. Soc.* **2020**, *167*, 110520.
- [40] Y. Dai, Y. Zhang, L. Gao, G. Xu, J. Xie, *Electrochem. Solid-State Lett.* **2010**, *13*, A22.

Manuscript received: October 10, 2022

Accepted manuscript online: November 6, 2022

Version of record online: December 7, 2022